Backside Absorbing Layer Microscopy: A universal relationship between physical thickness and reflectivity

Refahi Abou Khachfe, Dominique Ausserré

Backside Absorbing Layer Microscopy: A universal relationship between physical thickness and reflectivity

REFAHI ABOU KHACHFE[1] AND DOMINIQUE AUSSERRE[2]

[1] *Université libanaise, Faculté de technologie de Saida, Lebanon*
[1] *"Molecular Landscape, Biophotonic Horizons" group, Institut des Matériaux et Molécules du Mans UMR CNRS 6283, Le Mans Université, Avenue Olivier Messiaen, 72000 Le Mans, France*
**ausserre@univ-lemans.fr*

Abstract: The Backside Absorbing Layer Microscopy (BALM) is a recently introduced surface imaging technique in reflected light with an unprecedented combination of sensitivity and lateral resolution, hence very promising for the development of imaging sensors. This requires to turn BALM images into quantitative measurements. The usual way to analyze reflectivity measurements is to compare the optical signal and a numerical model with many adjustable parameters. Here we demonstrate a universal relationship between the sample reflectivity and the physical thickness of the sample, ruled by three measurable quantities. Mapping the true sample thickness becomes possible whatever the instrument configuration and the sample refractive index. Application to kinetic measurements is discussed.

1. Introduction

With the spreading of nanotechnology, there is an increasing need for ultrasensitive surface imaging techniques. Indeed, nano samples are most often supported on solid surfaces. This holds for all domains of application ranging from molecular electronics to diagnostics to biology to electrochemistry. In reflected light microscopy, anti-reflecting surfaces enhance the contrast of tiny objects by turning off the background reflectivity. This serves as a basis for a number of label free optical techniques [1-6]. Among them, the Backside Absorbing Layer Microscopy (BALM), a recent contrast technique in wide field optical microscopy [7,8], is especially promising. This reflected light microscopy lies on the use of special anti-reflecting layers as sample supporting plates. They are named ARA (meaning Anti-Reflecting and made of Absorbing materials). BALM offers the unmatched combination of a 200 nm optical resolution [3] and a SPR-like sensitivity (SPR = Surface Plasmon Resonance [5]). It is also remarkable for its simplicity and for its flexibility, since the top surface of the ARA coating can be of almost any nature and observed in any ambient medium using any reflected light microscope. The only requirement is to image the sample supported by the ARA coating from the opposite side of a thin transparent window on which it is deposited. The performance of the technique was already demonstrated by imaging 2D flakes of various materials [8], by following in situ and in real time their evolution upon small molecules adsorption and by detecting operando the electrochemical reduction of individual sub-10nm nanoparticles [9]. However, up to now the BALM images remained mainly qualitative [10] when characterization and sensing applications demand quantitative information. In the present work, we establish a universal relationship between the BALM reflectivity of a molecular layer sample and the physical thickness of this layer, with the two quantities made adimensional. This relationship can be used without any knowledge of the microscope settings or the ARA coating in order to obtain topographic AFM-like images of the sample,

whatever its complex refractive index, in a typical thickness range going from 0 to 30 nm. The thickness unit can be further determined with the help of a single reference measurement.

The most direct approach for a quantitative measurement consists in a comparison of the experimental data with a numerical calculation of the expected optical signal. It requires the adjustment of all the parameters affecting this signal. In the case of BALM, their number exceeds ten. Indeed, BALM is a white light, high aperture technique and there are many benefits to use ARA multi-layers made of two or three superimposed materials [11]. The modeling must take into account the spectral characteristics of the source and of the camera, all incidence angles contributing to the signal on the microscope, and one thickness and one complex refractive index per constitutive layer of the ARA coating. The comparison is heavy and risky. In addition, It must be redone for each BALM surface and each setup of the microscope. At the opposite of this "steam roller" procedure is the empirical approach, based on the comparison of the sample with a ruler made of regular steps imprinted on the same BALM substrate, allowing to map the local thickness. However, the reflectivity also depends on the refractive index of the sample, so it must be the same for the sample and the ruler, and this is a serious limitation. An alternative approach is to calibrate the optical measurement with a few AFM measurements on the same sample [11]. It has other drawbacks such as limitations on the nature of the sample or having to extract the sample from its environment in the optical setup, especially inconvenient when in a liquid. Here we present a new approach, which is equivalent in practice to replace the many above listed parameters by only three consolidated parameters (C-parameters), which are functions of the former ones but independent on the physical thickness of the sample. These C-parameters have a direct physical meaning when considering the BALM reflectivity $R(e)$ as a function of the sample thickness. Our approach is to expand $R(e)$ around its minimum. It takes advantage of two BALM specificities, namely the very low BALM reflectivity and the inverted ("backside") geometry. The mathematical existence of the minimum $R_{min}(e_{min})$ is granted by the low level, the continuity and the positive sign of $R(e)$. Yet e_{min} is not necessary positive. When negative, it is virtual. The inverted geometry allows direct analytical derivation of the sought expansion from a simple Fresnel theory. Limiting ourselves to the lower approximation level (second order), we end up with a universal relationship between an adimensional function of R and a reduced sample thickness, made adimensional as well. The two quantities are ruled case by case by the C-parameters which determine two scale factors acting along, respectively, the e and the R axis. A high constraint on $R(e)$ is the existence of a fixed point $[0, R_0]$, with $R_0 = R(0)$. R_0 is one C-parameter. It is experimentally accessible since it corresponds to the bare substrate. Depending on the application, several experimental strategies can be employed in order to determine the two other C-parameters e_{min} and R_{min}. Although a numerical estimating of these parameters is not forbidden, they are experimentally accessible. Then the thickness of the sample can be mapped without any information about the substrate or the microscope. Even the calibration with a known article becomes optional when the knowledge of the thickness unit is unimportant. As an example of application, we briefly envisage sensor-like kinetic studies.

2. Universal relationship

In this section, we show that BALM reflectivity can be approximated by a second degree polynomial of the sample thickness. After proper rescaling, it will become a universal function, with its square root a linear function of the thickness, hence a linear sensor. The rescaling involves 3 parameters which can quite easily be determined experimentally. Next we confront this rescaling with common process imaging tools. Finally, we show that the

method applies as well with continuous or discrete wavelength and/or incidence angle superposition. Figure 1 recalls the BALM geometry, and gives a visual support of the three parameters introduced.

In the Fresnel theory, the amplitude reflection coefficient of a multilayer [1,2,..., l] sandwiched between two semi-infinite media indexed by 0 and $l+1$ and lighted from material 0 is given by [12,13]:

$$r_{012\ldots l(l+1)} = \frac{r_{012\ldots l} + r_{l(l+1)} e^{-2j\beta_l}}{1 + r_{012\ldots l} r_{l(l+1)} e^{-2j\beta_l}} \quad (1)$$

with $r_{012\ldots l}$ the reflection coefficient of the l-1 first layers with the material l semi-infinite, $r_{l(l+1)}$ the Fresnel coefficient of the $l:(l+1)$ interface, $\beta_l = (2\pi e_l/\lambda)(n_l - jk_l)cos\theta_l$ the phase factor in layer l, λ the wavelength of light, e_l and $n_l - jk_l$ the thickness and complex refractive index of layer l and $cos\theta_l$ the angle of refraction in that layer. In imaging and sensing applications based on reflectivity, the probed layer can be either layer 1, we call it the upright geometry, or layer l, we call it the inverted geometry. Eq. (1) gives a special status to the last layer. The BALM measurement envisaged herein consists in extracting the physical thickness of the last layer from the (complex) amplitude coefficient given by Eq. (1). The two terms $r_{012\ldots l}$ and $r_{l(l+1)}$ are functions of the refractive index of the probed layer, and β_l is a function of both its refractive index and thickness. A complex reflection coefficient r cannot be directly probed from a reflectance measurement. What is measured is $R = |r|^2$. In general, β_l is a complex number. On the understanding that we talk about the last layer in the stack, we will most often neglect the l index. Setting $\beta = \beta_{\mathcal{R}} - j\beta_{\mathfrak{I}}$ and expanding R to second order in $\beta_{\mathcal{R}}$ and $\beta_{\mathfrak{I}}$, we find:

$$R = R_0\left[1 + A\beta_{\mathfrak{I}} + B\beta_{\mathcal{R}} + C{\beta_{\mathfrak{I}}}^2 + D\beta_{\mathcal{R}}\beta_{\mathfrak{I}} + E{\beta_{\mathcal{R}}}^2\right] \quad (2)$$

, with $R_0 = \left|r_{012\ldots(l-1)(l+1)}\right|^2$ the bare substrate reflectivity, corresponding to $\beta_l = 0$ in Eq. (1), and the polynomial coefficients A, B, C, D, E (not made explicit here) independent of e. The relative reflectivity change with the presence of the probed layer is:

$$\frac{R - R_0}{R_0} = Ue + Ve^2 \quad (3)$$

, with U and V independent of e. Eq. (3) shows thickness and index separability, which somehow contrasts with the intuitive belief that the optical thickness obtained from optical interference measurements cannot be split into the two parts. Indeed, Eq. (3) expresses the reflectivity as a parabolic expression of the true thickness e, the dependence of R with n and k being confined within the two coefficients $U = 2\pi cos\theta(Ak + Bn)/\lambda$ and $V = (2\pi cos\theta)^2(Ck^2 + Dnk + En^2)/\lambda^2$. Even when the probed layer is non absorbing, i.e. $k = 0$, we cannot merge n with e because A, B, C, D, E depend on n via the Fresnel and multilayer reflection coefficients. In a sensing or a sensitive imaging experiment, what is demanded is a maximal optical sensitivity to the presence of the upper layer l. This is obtained when the reflectivity of the substrate is very low. Therefore, the reflectivity given by Eq. (3) is close to its minimum value R_{min} with respect to e, obtained when $e = e_{min}$. From Eq. (3), $e_{min} = -U/2V$ and $(R_{min} - R_0)/R_0 = -U^2/4V = Ue_{min}/2$. Straightforward algebra gives ($U \neq 0$):

$$\frac{R - R_{min}}{R_0 - R_{min}} = \left(\frac{e - e_{min}}{e_{min}}\right)^2 \quad (4)$$

The two parameters e_{min} and R_{min} act as two scale factors in a universal relationship. Whatever the nature of the substrate, Eq. (4) will apply. It will only affect R_0 and the two unknown scale factors. Once the three C-parameters associated to the BALM surface and the instrument determined, it will deliver thickness measurements everywhere on the same surface, with the thickness unit as the only missing information. When mapping in plane or in time thickness variations of a surface layer, it is a considerable intake when the intensity in the image is proportional to the local thickness. Thus we reformulate Eq. (4) as :

$$\left|\frac{e-e_{min}}{e_{min}}\right| \cong f\left(\frac{R}{R_{min}}, \frac{R_0}{R_{min}}\right) \quad (5)$$

, with $f(R/R_{min}, R_0/R_{min}) = \sqrt{(R-R_{min})/(R_0-R_{min})}$. When unambiguous, we will refer to this function as $f(R)$. The sign uncertainty in Eq. (5) is resolved with $e/e_{min} = 1 + sgn[e_{min}(e-e_{min})]f(R)$.

With optical microscopy, an important issue is image contrast. Optimizing the brightness/contrast of the desired patterns with numerical tools consists in changing the raw intensity distribution $I(x,y)$ for a more readable image $J(x,y)$ according to the affine transform $(x,y) = q_1 I(x,y) + q_2$, with q_1 and q_2 arbitrary real numbers. Applied to BALM images, the true reflectivity R is thus changed for some displayed reflectivity $R' = q_1 R + q_2$. The affine transform affects all the terms in the left member of Eq. (4), and we get $(R' - R_{min}')/(R_0' - R_{min}') = [((e-e_{min})/e_{min})^2]$, with the right member unchanged. This remark is of a high practical importance: it says that the measurements can be performed as well on brightness/contrast transformed images, and that display optimization of BALM images or videos and quantitative BALM analysis are fully compatible. Notice that following the affine transform, R_{min}' may become negative. A very interesting situation is to work with an (initially) negative contrast and to have R_{min}, hence inversion of the reflectivity variation with e, appearing somewhere in the image. Then, suppressing all the levels under R_{min} in the histogram will set R_{min}' to zero. In that case $f(R)$ reduces to $\sqrt{R'/R_0'}$ and the square root of the image is a true topographic image, with the intensity everywhere proportional to the thickness of the layer, but with a slope inversion at $[e_{min}, 0]$. Instead of calculating the square root of the image, one can equivalently apply a 0.5 gamma correction.

In order to convert the reflectivity into a thickness, the sign in Eq. (5) must be identified. It relies in general on ordering the local reflectivity values in the image, or simply on the appropriate choice of the BALM substrate. The thickness e_{min} is positive when the contrast of the burgeoning layer l with the bare substrate is negative, and it is negative with a positive contrast, becoming an extrapolated length. With e_{min} positive, the contrast decreases with e up to $e = e_{min}$ and increases afterwards. Then, to a given value of R correspond two possible values of the thickness, which are symmetric on each part of e_{min}. The symmetry can be broken by changing the color of the lighting. Indeed, e_{min} depends on this choice. Here we take advantage of the compatibility of the BALM with white light. It is therefore important to examine the effect of color (wavelength) averaging on the measurements. We will envisage at the same time incidence angle averaging, which conditions lateral resolution. Starting again from Eq. (3), the reflectivity can be expressed for a given wavelength and incidence angle as $R(\theta,\lambda) = R_0(\theta,\lambda) + [R_0(\theta,\lambda)U(\theta,\lambda)/\lambda]e + [R_0(\theta,\lambda)V(\theta,\lambda)/\lambda^2]e^2$. Assuming incoherent superimposition of all angle and wavelength contributions, we get :

$$\langle R\rangle_{\theta,\lambda} = \langle R_0\rangle_{\theta,\lambda} + \langle\frac{R_0 U}{\lambda}\rangle_{\theta,\lambda} e + \langle\frac{R_0 V}{\lambda^2}\rangle_{\theta,\lambda} e^2 \quad (6)$$

The averaged reflectivity is a polynomial of e similar to Eq. (3), so we can directly write:

$$\frac{\langle R\rangle_{\theta,\lambda}-R_{min_{eff}}}{\langle R_0\rangle_{\theta,\lambda}-R_{min_{eff}}}=\left(\frac{e-e_{min_{eff}}}{e_{min_{eff}}}\right)^2 \tag{7}$$

with $e_{min_{eff}}$ and $R_{min_{eff}}$ the effective coordinates of the minimum with the averaged reflectivity. The important point is that Eq. (4) applies again. The measurement of e can be performed with any lighting spectrum and with any microscope aperture, provided that the contrast remains sufficient.

3. Model cases and discussion

Next we make things more concrete by considering three ARA configurations which are particularly relevant for the design of BALM imaging sensors. The first one is the glass/gold/*n2*/water stack, or GAn_2W. It is interesting because the gold sensing surface allows direct comparison with SPR, the gold technique in the study of bio-molecular interactions. The second one is glass/gold/silica/*n3*/water, or GASn_3W which extends the BALM imaging sensor to the silica surface, the gold standard in surface chemistry. The third one is glass/gold/graphene oxide/n_3/water, or GAGOn_3W, one of the most promising combination for BALM ultra-high density multi-array diagnostics.

3.1 Gold substrate

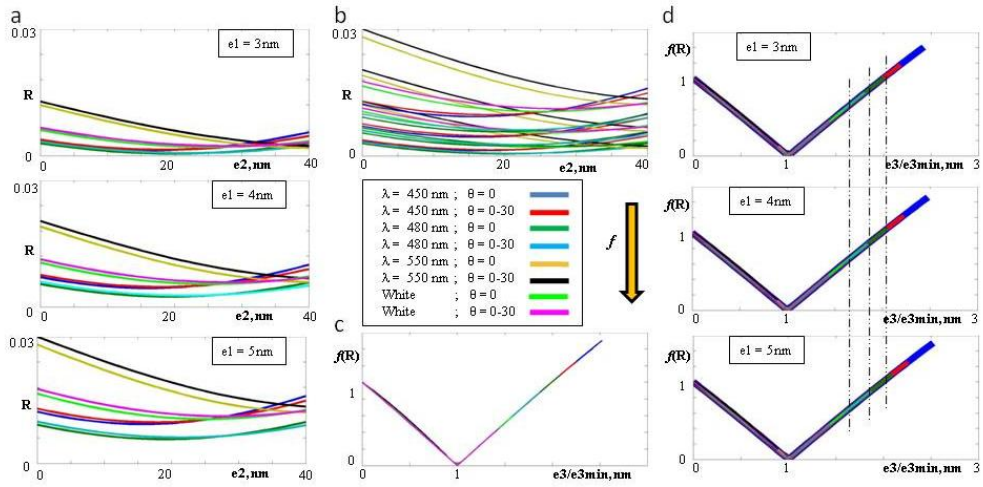

Figure 1 a): Reflectivity as a function of the sample thickness for 24 configurations : [e_1 = 3, 4 and 5 nm (gold)] x [λ=450, 480, 550 nm and 3*1/3 average ("white")] x [θ = 0 or 30 deg. aperture angle], with one graph per thickness; b): same with the 24 superimposed results; c): transformed reflectivity $f(R/R_{min}, R_0/R_{min})$, noted $f(R)$, as a function of the reduced sample thickness e/e_{min}, with different e_{min}, R_{min} and R_0 for each parameter configuration; d): same curve as c) with each thickness isolated and the corresponding e/e_{min} range compared to each other using dotted lines; Figure insert : color code for each (λ, aperture) setting. The refractive indices n_0, n_2, n_3, weakly dependent of λ, are respectively fixed to 1.52, 1.5 and 1.34, and n_1 *(λ)* was taken from [14].

Figure 1a displays the reflectivity curves $R(e_2)$ expected with a GAn_2W BALM substrate with fixed $n_0 = 1.52$ (glass) and $n_2 = 1.5$ (sample). They were numerically computed for three different values of the gold layer thickness, for three different wavelengths and for the two lighting configurations of a normal incidence and of a uniform illumination cone with a

30 degrees apex semi-angle (angle averaging). We also included wavelength average, referred to as "white", by adding with equal weight the contributions of three wavelengths. 450 nm, 480 nm and 550 nm. Superimposing all cases, we obtain in Figure 1b a forest of 24 different graphs without apparent correlation between them. In each case we extract the value of the three C-parameters $[R_0, e_{min}, R_{min}]$ and we plot the graph $[e/e_{min}, f(R)]$. The result is shown in Figure 1c. All previous graphs merge in a single curve made of two orthogonal line segments with slope -1 and +1, crossing at $[1, 0]$. This figure illustrates how the entire reflectivity analysis resumes in the determination of the three C-parameters. Figure 1d clarifies with the help of color correspondences the partial covering of the universal curve specific to each configuration. We previously mentioned that e_{min} can be positive as it the case in Figure 1 or negative. It may also be zero, making Eq. (4) and subsequent equations ill-defined. It corresponds to $U = 0$ in Eq. (3), $R_0 = R_{min}$, and $(R - R_{min})/R_{min} = Ve^2$. In this special case, $f(R) = \sqrt{R/R_{min} - 1}$ and the scaling factor for e is $\sqrt{V}$ in place of e_{min}. In the left part of Figure 1c, small deviations with respect to Eq. (4) (or equivalent Eq. (7)) are observed. They correspond to the case $e_1 = 5$ nm where e_{min} is large and where the second order approximation reaches its limits. When needed, the expansion of $f(R)$ can be extended to next orders in $\left(e - e_{min_{eff}}\right)/e_{min_{eff}}$ while keeping all variables adimensional, allowing to reproduce curve asymmetry and inflexion points for larger sample thickness. These developments are beyond our present scope.

3.6 Silica substrate

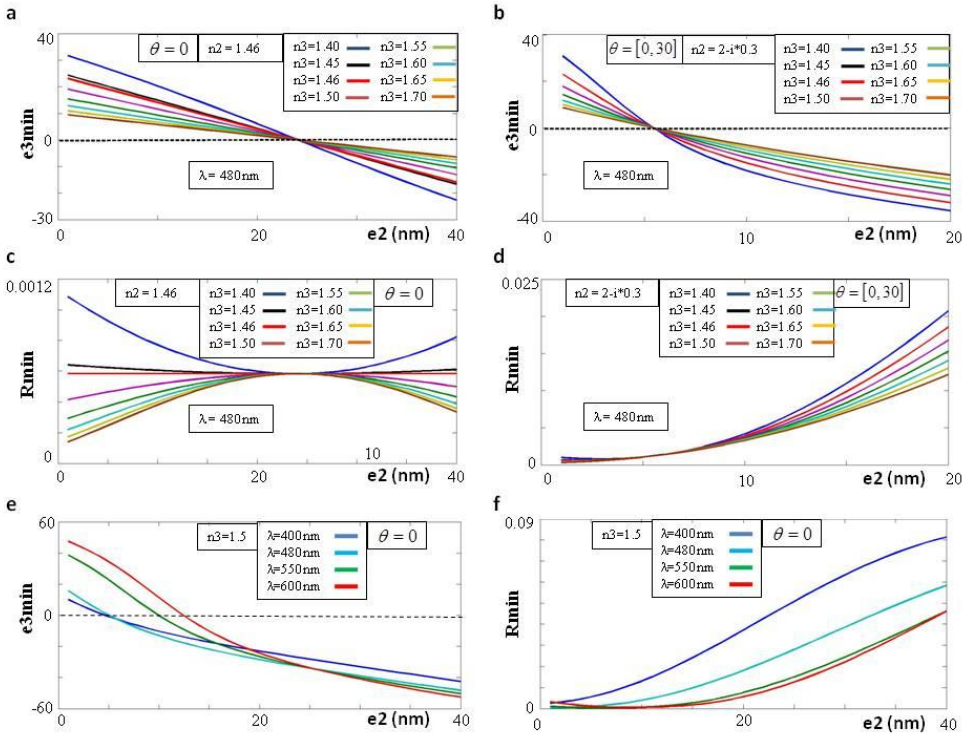

Figure 2 a), c) : GAS*n3*W, θ = 0 ; b),d): GAGO*n3*W and illumination cone $\theta = 0 - 30$ deg. a),b): e_{3min}(probed layer) as a function of e_2 for a number of n_3 refractive indices ranging from 1.4 to 1.7; c),d): R_{min} as a function of e_2 for the same n_3 values; e),f) GAGO*n3*W with $\theta = 0$ and e_1= 3nm (gold). e_{3min} and R_{min} as a function of e_2 (GO)

for four different wavelengths; inserts: color codes for the sample refractive index in 2a-d and for the wavelength in 2e-f. The GO refractive index as a function of λ was taken from [15].

In Figure 2, the gold layer thickness was fixed to 3 nm. In Figures 2a and 2c, we envisage the second case, GASn_3W and we chose normal incidence. According to what precedes, the detailed reflectivity curves are useless. Only matters the value of the three C-parameters. With a given substrate, GAS and W are fixed in GASn_3W, thus R_0 is fixed. It is obtained for $e_3 = 0$ and does not depend on n_3, the zero thickness meaning no layer. Figure 2a shows the variation of e_{3min} with the thickness e_2 of the silica layer for a number of refractive indices n_3. It is monotonic. A straight line with a slope -1 is obtained when $n_3 = n_2$, meaning that a variation of e_3 and the opposite variation of e_2 are equivalent. With this stack, e_{3min} goes from positive to negative, depending on the e_2 value. It covers the case $e_{3min} = 0$, marked by a fixed point in the batch of n_3-curves in Figure 2a because the absence of layer is insensitive to its refractive index. The corresponding value of e_2 is 24 nm. Figure 2c shows the variation with e_2 of R_{3min} (minimum of R vs e_3). It also exhibits a fixed point with a zero slope in correspondence with $e_{3min}(e_2) = 0$, i.-e. when $e_2 = 24$ nm. As for e_{3min}, the existence of the fixed point corresponds to the absence of the n_3 layer. The zero slope is explained by similar yet less direct arguments as for the existence of the fixed point. We do not dwell on it. A first order transition on the sign of the curvature around this extremum is observed for $n_3 = 1.46$. It corresponds to the change of the phase sign at the $n_2{:}n_3$ interface. Figures 2b and 2d show equivalent variations $e_{3min} = f(e_2)$ and $R_{min} = f(e_2)$ in the case of the GAGOn_3W stack. In Figures 2b and 2d we chose a 30 deg. microscope aperture, aiming to illustrate the flexibility of our approach. They present a number of common features with Figures 2a and 2c, in particular the existence of the fixed points, here for $e_2 = 5{,}4$ nm . The deviation with the straight line on $e_{3min} = f(e_2)$ and the deviation with the zero slope on $R_{min} = f(e_2)$ are due the 0.3 absorption coefficient of the GO layer, making $n_3 = n_2$ impossible. Due to the same, the value of R_{min} becomes too high ($> 10^{-2}$) when the GO thickness reaches 10 or 15 nm, while it is of order 10^{-3} when e_2 is under 8 nm. Figures 2a to 2d underline with indexed color curves the important variations of e_{min} and R_{min} with the sample refractive index away from the fixed point, bringing interesting possibilities for estimating n_3. Figures 2e and 2f at least illustrate the strong dependence of $e_{min}(e_2)$ and $R_{min}(e_2)$ with wavelength expected with GAGOn_3W for $e_1 = 3nm$, which opens promising possibilities for multispectral measurements.

3.6 Graphene Oxide spot

Figure 3 at least focuses on a major BALM application which is investigation of (bio)molecular interactions through capture, dissociation or exchange kinetic studies. For illustration, we consider the $GAGOn_3W$ stack, where GO flakes are considered the probe spots. For the sake of simplicity, we envisage only one layer fixing on the GO surface, with refractive index 1.5. We chose 3 nm and 2 nm for respectively the Au and the GO thickness because it makes a good compromise between negative contrast ($e_{3min} > 0$), high sensitivity and ease of manufacture. We also fix $\lambda = 480\ nm$, the most sensitive wavelength with the gold layer [7] and we consider both a normal incidence and a 30 degrees microscope aperture. In presence of the target solution, the growth of the target layer (e_3, n_3) on GO is revealed by the time dependent reflectivity $R[e_3(t)]$. It is linked to the true layer thickness by Eq. (4). e_{min} positive is an essential asset in the kinetic studies because, in addition to bare substrate reflectivity R_0, the parameter R_{min} is experimentally determined, the curve $R[e_3(t)]$ covered during the kinetics passing through the minimum $[t(e_{min}), R_{min}]$. Figure 3c shows a canonical kinetics $e_3(t) = e_3(\infty)\left(1 - e^{-t/\tau}\right)$, with $e_3(\infty)$ the saturation thickness fixed to 25 nm and τ the undefined characteristic time of the capture process. Figures 3a and 3e show the corresponding evolution of the BALM reflectivity, respectively calculated for a normal

incidence and for a 30 deg. aperture. In each case, R_{min} and $t(e_{min})$ are extracted. Figures 3b and 3f are obtained from Figures 3a and 3e by applying the transform $R \rightarrow f(R/R_{min}, R_0/R_{min})$, with a careful attention paid to the sign. Although R is a function of t, the transform automatically yields the two straight lines displayed in Figures 3b and 3f, a universal function of $e(t)/e_{min}(t)$ independent of t. In other words, the curve in Figure 3b or 3f is always the same, parameterized by t. t rules the speed at which the curve is explored but does not impact its shape. From Figures 3b or 3f, we get the result $t(e/e_{min})$ shown in Figure 3d when replacing $f[R(t)]$ by the corresponding value of t.

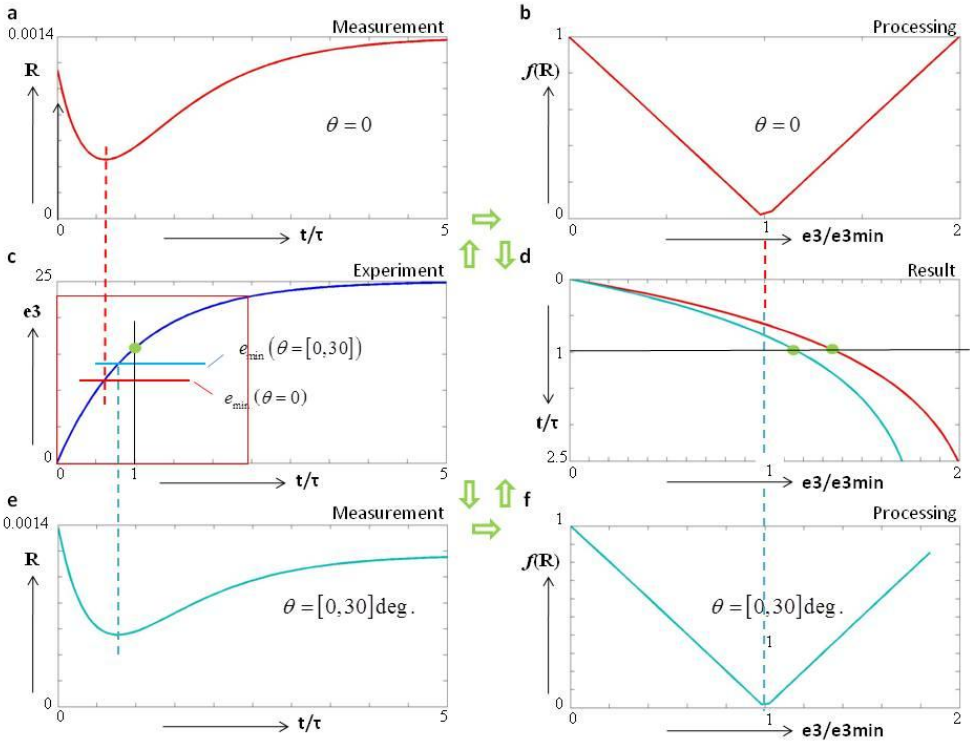

Figure 3 Schematic sequence of a kinetic experiment. The green arrows show two measurement and analysis sequences with two different illuminations. c) postulated kinetics $e_3(t/\tau)$; a) Simulated experimental reflectivity $R(t/\tau)$ for a normal incidence; e) Simulated reflectivity $R(t/\tau)$ for a 30 deg. aperture; b) $f(R)$ as a function of e/e_{min} resulting from the transform of a); e) same with the transform of e); d) measured kinetics $(t/\tau)(e_3)$ obtained from a) and b) or from e) and f); fixed values $e1$=3 nm (gold) and $e2$ = 2 nm (GO).

In Figure 3, the two sequences corresponding to the two aperture settings are highlighted by the green arrows. The C-parameters R_0, e_{min} and R_{min} are different in each case but the process and the result are the same, apart for the unknown thickness unit, which case by case determination requires a caliber or a single external measurement. The comparison of the two sequences illustrates with the aperture example how we save the adjustment of experimental parameters. Incidentally, it also illustrates the weak sensitivity of BALM to numerical aperture, which is the cornerstone of the BALM potential in imaging sensor applications. To be practical, nothing but the presence of noise would be different with a real kinetic in Figure 3c. The BALM experiment would deliver Figures 3a or 3e, and Figure 3d would be directly obtained from the transform $(f^{\circ}R)^{-1}(t)$. For a 90° rotation, it reproduces the real kinetics of Figure 3b. Thus, Figures 3b or 3f have mainly a pedagogical virtue. Whatever the experimental conditions, the characteristic time τ would be obtained from the time dependent

reflectivity without any calibration. Measurement of the saturation level $e_3(\infty)$ would require the help of a single thickness caliber.

4. Conclusion

To step back from the above examples, the aim of our approach is to introduce three consolidated "C-parameters" in replacement of the multiple parameters to consider when fitting the experimental curve with a model. The former ones are functions of the latter, and constitute an intermediate stage between influencing parameters and analysis. Studying the dependence of the C-parameters with some others is a useful route for many purposes such as instrument optimization, substrate design and characterization or refractive index measurement. On the other hand, using the C-parameters in order to obtain the true "AFM-like" topography of a sub-nanometer thick sample film is immediate and effective with very little effort. In the numerical examples presented above, we have only envisaged purely transparent, i.-e. non absorbing sample layers. The case of absorbing layers was addressed in [11]. The high sensitivity of e_{min} on k_3 was demonstrated, which confirms possibilities for molecular layer characterization. We do not insist here on the refractive index analysis, since our present focus is to introduce the universal relationship between reflectivity and physical thickness as a basis for quantitative BALM measurements. Application to real experiments will follow with SPRi-like kinetic studies and monolayer counting in 2D material flakes.

References

1. T.Sandström, M.Stenberg, H. Nygren "Visual detection of organic molecular films b interference colors" Appl. Opt. **24**, 472-479 (1985)
2. K. S. Novoselov, A. K. Geim, S. V. Morozov, D. Jiang, Y. Zhang, S. V. Dubonos, I. V. Grigorieva and A. A. Firsov, "Electric Field Effect in Atomically Thin Carbon Films" Science **306**, 666-669 (2004)
3. D. Bing, Y. Wang, J. Bai, R. Du, G. Wu and L. Liu, " Optical contrast for identifying the thickness of two-dimensional materials" Optics Communications **406**, 128-138 (2018)
4. D. Ausserré and M-.P. Valignat "Wide-Field Optical Imaging of Surface Nanostructures" NANO LETTERS **6**(7), 1384-1388 (2006)
5. Hoang Hiep Nguyen, Jeho Park, Sebyung Kang , and Moonil Kim "Surface Plasmon Resonance: A Versatile Technique for Biosensor Applications" Sensors **15**, 10481-10510 (2015); doi:10.3390/s150510481
6. Ugur Aygun, Oguzhan Avci, Elif Seymour, Hakan Urey, M. Selim Ünlü and Ayca Yalcin Ozkumur "Label - Free and High-Throughput Detection of Biomolecular Interactions Using a Flatbed Scanner Biosensor"ACS Sens. 20172101424-1429 (2017); doi.org/10.1021/acssensors.7b00263
7. D. Ausserre, C. Amra, R. Abou Khachfe, L. Roussille, G. Brotons, L. Vonna, F. Lemarchand and M. Zerrad "Anti-Reflecting Absorbing Layers for Electrochemical and Biophotonic Applications" Journal of Nanomedicine & Nanotechnology **5**, 1000214 (2014)
8. S. Campidelli, R. Abou Khachfe, K. Jaouen, J. Monteiller, C. Amra, M. Zerrad, R. Cornut, V. Derycke and D. Ausserré "Backside absorbing layer microscopy: Watching graphene chemistry" Science Advances **3**, e1601724 (2017)
9. Jean-Francois lemineur, Jean-Marc Noël, Dominique Ausserré, Catherine Combellas, Frederic Kanoufi "Combining electrodeposition and optical microscopy for probing size-dependent single nanoparticle electrochemistry" Angewandte Chemie, Communication 57(37) 11998-12002 (2018); https://doi.org/10.1002/anie.201807003
10. http://www.watchlive.fr/ taken on 2019, june 20th.
11. K. Jaouen, R. Cornut, D. Ausserré, S. Campidelli,V. Derycke, " Ideal optical contrast for 2D materials observation using bi-layer antireflection absorbing substrates" Nanoscale **11**(13):6129-6135 (2019); doi: 10.1039/c8nr09983a
12. L. G. Parratt " Surface Studies of Solids by Total Reflection of X-Rays" Phys. Rev. **95**(2) 359 (1954)
13. R. M. A. Azzam, N. M. Bashara, "Ellipsometry and polarized light" , ISBN North-Holland 0 7204 0694 3, (1977).
14. P. B. Johnson and R. W. Christy, "Optical constants of the noble metals," Phys. Rev. B 6, 4370 (1972).

15. V. G. Kravets,, O. P. Marshall, R. R. Nair, B. Thackray, A. Zhukov, J. Leng, and A. N. Rigorenko "Engineering optical properties of a graphene oxide metamaterial assembled in microfluidic channels" optics express **32**(2), (2015)